Forbidden nonunique β decays and effective values of weak coupling constants

M. Haaranen,[1] P. C. Srivastava,[2] and J. Suhonen[1]
[1]*University of Jyväskylä, Department of Physics, P.O. Box 35 (YFL), FI-40014, University of Jyväskylä, Finland*
[2]*Department of Physics, Indian Institute of Technology, Roorkee 247667, India*
(Received 28 October 2015; revised manuscript received 22 January 2016; published 8 March 2016)

Forbidden nonunique β decays feature shape functions that are complicated combinations of different nuclear matrix elements and phase-space factors. Furthermore, they depend in a very nontrivial way on the values of the weak coupling constants, $g_{\rm V}$ for the vector part and $g_{\rm A}$ for the axial-vector part. In this work we include also the usually omitted second-order terms in the shape functions to see their effect on the computed decay half-lives and electron spectra (β spectra). As examples we study the fourth-forbidden nonunique ground-state-to-ground-state β^- decay branches of ^{113}Cd and ^{115}In using the microscopic quasiparticle-phonon model and the nuclear shell model. A striking new feature that is reported in this paper is that the calculated shape of the β spectrum is quite sensitive to the values of $g_{\rm V}$ and $g_{\rm A}$ and hence comparison of the calculated with the measured spectrum shape opens a way to determine the values of these coupling constants. This article is designed to show the power of this comparison, coined spectrum-shape method (SSM), by studying the two exemplary β transitions within two different nuclear-structure frameworks. While the SSM seems to confine the $g_{\rm V}$ values close to the canonical value $g_{\rm V} = 1.0$, the values of $g_{\rm A}$ extracted from the half-life data and by the SSM emerge contradictory in the present calculations. This calls for improved nuclear-structure calculations and more measured data to systematically employ SSM for determination of the effective value of $g_{\rm A}$ in the future.

DOI: 10.1103/PhysRevC.93.034308

I. INTRODUCTION

The problem related to the value of the axial-vector coupling constant $g_{\rm A}$ is an old and well-known one. The constant $g_{\rm A}$ enters the β-decay theory as means of re-normalizing the hadronic current of the decaying nucleus [1,2]. Part of this re-normalization comes from the nonnucleonic degrees of freedom [3] and part from the nuclear many-body effects as discussed below. The β-decay rates contain $g_{\rm A}$ up to the second power whereas the double-β-decay rates contain $g_{\rm A}$ up to the fourth power [4,5]. Thus it is of great importance to have a good understanding of the value of $g_{\rm A}$ when assessing the potential experimental verification of the neutrinoless mode of double β decay (check, e.g., Refs. [6,7]).

Although the so-called bare nucleon value, roughly $g_{\rm A} = 1.25$, can readily be derived from theoretical considerations, i.e., from the partially conserved vector current (PCVC) hypothesis of the standard model [8], there are reasons to suspect that this is not the appropriate value when working inside the nuclear matter and finite nuclei. The attempts to probe the value of $g_{\rm A}$ have been done mainly in the context of the proton-neutron quasiparticle random-phase approximation (pnQRPA) [6,7,9–13], the nuclear shell model (NSM) [14–16], and the interacting boson approximation (IBA) [17,18]. These studies have compared the measured data with the corresponding computed observables in the context of allowed and first-forbidden unique β decays, as well as two-neutrino double β decays. All these studies show consistently that $g_{\rm A}$ has to be (considerably) quenched in the calculations to match the wide set of data used in the analyses. This quenching can be partly explained by the nonnucleonic degrees of freedom that remove some strength from the low-lying nuclear excitations [3] and partly by the nuclear many-body effects: truncations in the single-particle model space and/or deficiencies in the treatment of the many-body quantum mechanics. There are also some specific problems like the $g_{\rm pp}$ problem of the pnQRPA [19] that makes the determination of the value of $g_{\rm A}$ somewhat problematic. Limitations of the various models have been discussed, e.g., in Ref. [20].

The discussion about the quenching of $g_{\rm A}$, or its effective value, has recently been boosted by the attempts to calculate the nuclear matrix elements related to the neutrinoless double β decay. Because the decay rate of this decay mode depends on the fourth power of $g_{\rm A}$ it is of paramount importance to know the effective value of this quantity in a nucleus. There is no theory yet which would tell how the effective value of $g_{\rm A}$, as probed in β decays and two-neutrino double β decays, connects to the one of the neutrinoless double β decays. The differences in the mentioned decays stem from the quite different magnitudes of the exchanged momenta and the different structure of the decay operators (the neutrinoless double β decay includes additional neutrino potentials in the transition operators from the propagation of the virtual neutrino between the two decaying nucleons). Because the neutrinoless double β decay can contain momentum exchanges roughly up to 100 MeV, the higher-forbidden channels ($0^+ \to 2^+,3^+,3^-,4^+,4^-$, etc.) are not much suppressed against the allowed ($0^+ \to 0^+,1^+$) and first-forbidden ($0^+ \to 0^-,1^-,2^-$) channels. This makes the present study important: Are the higher-forbidden transitions suppressed by the effective value of $g_{\rm A}$ or not? The high-forbidden β decays are a unique chance to attack this problem and here we concentrate on two exemplary fourth-forbidden transitions.

The conserved vector current (CVC) hypothesis protects the value of the vector coupling constant $g_{\rm V} = 1.0$ [8]. However, like $g_{\rm A}$, $g_{\rm V}$ could attain effective values in practical nuclear-structure calculations, pertaining to various truncations in the nuclear many-body problem. Quenched values of $g_{\rm V}$ were early on obtained in extensive shell-model calculations

of spin-dipole and first-forbidden β transitions in the lead region [21,22]. In the more recent calculations [23,24] this analysis was extended to $N = 80,82,126$ nuclei by comparing the available data with shell-model calculations for Gamow-Teller and first-forbidden β-decay rates. The obtained quenchings for $g_{\rm V}$ were sizable. It is thus of great interest to see if such quenching pertains to higher-forbidden β transitions, and in particular can the quenching be seen in the β spectrum of a given high-forbidden β transition. Inspired by these observations, we further extended the present spectrum-shape method (SSM) analysis to probe the possible effects of the vector coupling. Thus in the current work the computed results are subject to the potential quenching of both $g_{\rm V}$ and $g_{\rm A}$.

Referring to the above discussion, we want to inspect the role of the weak coupling constants $g_{\rm V}$ and $g_{\rm A}$ in the ground-state-to-ground-state β decays of ^{113}Cd and ^{115}In. Both of these are fourth forbidden nonunique transitions with partial half-lives $t^{\beta}_{1/2} = (8.04 \pm 0.05)\times 10^{15}$ yr and $t^{\beta}_{1/2} = (4.41 \pm 0.25)\times 10^{14}$ yr, respectively [25]. These decays were previously studied in Ref. [26], and in the current work we revisit the same subject. More notably, we present two different methods for the extraction of the effective value of $g_{\rm A}$ from the experimental data. At the same time we aim at exploring the effects of $g_{\rm V}$ on the decay half-life and β spectrum. We extend the previous study [26] by performing the calculations with two different nuclear models, namely the microscopic quasiparticle-phonon model (MQPM) [27] and the nuclear shell model (NSM). For the latter we use the code NUSHELLX [28]. In addition, we also inspect the contributions that stem from the previously unaccounted-for second-order terms of the β-decay shape function. Finally, we also want to point here to the sensitivity of the computed β spectrum to the values of $g_{\rm V}$ and $g_{\rm A}$. This feature was overlooked in [26].

The first method for probing the value of $g_{\rm A}$ is the straightforward comparison of the theoretically computed partial half-life with the experiment. In the current work this is implemented by plotting the partial half-life values as functions of the effective value of $g_{\rm A}$. The second method is a completely new approach, and it utilizes the dependence of the computed β-spectrum shape on the value of $g_{\rm A}$. By plotting the computed β spectra for different values of $g_{\rm A}$ we have noticed that the dependence of the spectrum on the effective value of $g_{\rm A}$ can be very strong. This raises the intriguing question of how the effective value of $g_{\rm A}$ can be extracted by using this strong dependence. The obvious way to do this is to compare with experimental data, in this particular case with the spectrum shape extracted by Belli *et al.* [29] for ^{113}Cd. This comparison we coin the spectrum-shape method. In the same way we can extend the half-life and SSM analyses to take into account the effect of a possible quenching in the value of the vector coupling constant $g_{\rm V}$.

This article is organized as follows. In Sec. II we give a short overview on the theoretical formalism. We concentrate mainly on the theory of forbidden β decays and describe some of the basic principles involved. This formalism was previously applied to the studies of such decays, e.g., in Refs. [30–32]. We do not discuss the properties and details of the two nuclear models in the current work but rather refer the reader to take a look at, e.g., [27] for the MQPM and [33] for the NSM. In Sec. III we lay out the numerical background of the calculations and in Sec. IV we present the results of our calculations and perform the comparison with experimental data. Finally, in Sec. V we draw the conclusions.

II. THEORETICAL FORMALISM

The general theoretical formalism for the β-decay process in the context of both allowed and forbidden types of decays is described in full detail in Ref. [2] (check also Ref. [1]). Based on this thorough treatment of the subject a more streamlined discussion concentrating on the practical aspects of the theory can be found, e.g., in Ref. [34]. It is worth noting, however, that Ref. [34] does not discuss the second-order terms of the shape factor, included in this work.

When the β^--decay process is described as a pointlike interaction vertex with an effective coupling constant $G_{\rm F}$, the Fermi coupling constant, the probability for the electron to be emitted in the energy interval $W_{\rm e}$ to $W_{\rm e} + dW_{\rm e}$ is given by

$$P(W_e)dW_{\rm e} = \frac{G_{\rm F}^2}{(\hbar c)^6}\frac{1}{2\pi^3\hbar}C(W_{\rm e}) \times p_{\rm e}cW_{\rm e}(W_0 - W_{\rm e})^2 F_0(Z,W_{\rm e})dW_{\rm e}. \quad (1)$$

The quantity $p_{\rm e}$ in Eq. (1) is the electron momentum and W_0 is the end-point energy of the β spectrum corresponding to the maximum electron energy in the decay transition. The function $F_0(Z,W_{\rm e})$ is the Fermi function for β^- decays [see Eq. (32) in Ref. [34]] and Z is the proton number of the daughter nucleus.

To render the subsequent derivations more convenient and systematic a set of unitless kinematic quantities is usually introduced. These quantities are $w_{\rm e} = W_{\rm e}/m_{\rm e}c^2$, $w_0 = W_0/m_{\rm e}c^2$, and $p = p_{\rm e}c/m_{\rm e}c^2$, i.e., the ones appearing in Eq. (1) divided by the electron rest-mass energy $m_{\rm e}c^2$. Using this convention the partial half-life of the decay can be expressed as $t_{1/2} = \kappa/\tilde{C}$, where the constant,

$$\kappa = \frac{2\pi^2\hbar\ln 2}{(m_{\rm e}c^2)^5 G_{\rm F}^2/(\hbar c)^6}, \quad (2)$$

and the unitless integrated shape factor is defined as

$$\tilde{C} = \int_1^{w_0} C(w_{\rm e})pw_{\rm e}(w_0 - w_{\rm e})^2 F_0(Z,w_{\rm e})dw_{\rm e}. \quad (3)$$

Nuclear-structure information, and hence, the characteristics of the decay are contained in the shape factor of Eq. (3). The general expression for this factor is given by

$$C(w_{\rm e}) = \sum_{k_{\rm e},k_\nu,K} \lambda_{k_{\rm e}}(M_K(k_{\rm e},k_\nu)^2 + m_K(k_{\rm e},k_\nu)^2 - \frac{2\gamma_{k_{\rm e}}}{k_{\rm e}w_{\rm e}}M_K(k_{\rm e},k_\nu)m_K(k_{\rm e},k_\nu)), \quad (4)$$

where the terms $M_K(k_{\rm e},k_\nu)$ and $m_K(k_{\rm e},k_\nu)$ are complicated combinations of kinematic factors and nuclear form factors. The quantity $\gamma_{k_{\rm e}} = \sqrt{k_{\rm e}^2 - (\alpha Z)^2}$ and $\lambda_{k_{\rm e}} = F_{k_{\rm e}-1}(Z,w_{\rm e})/F_0(Z,w_{\rm e})$, where $F_{k_{\rm e}-1}(Z,w_{\rm e})$ is the generalized Fermi function. The positive integers $k_{\rm e}$ and k_ν are related to the partial wave expansions of the electron (e) and neutrino (ν) wave functions.

In impulse approximation the decaying nucleus is independent of the rest of the nucleons. The other nucleons act only as spectators, and thus the meson exchange and other many-body effects are neglected. The form factors themselves can be expanded as power series of the quantity $qR/\hbar$, where q is the neutrino momentum and R the nuclear radius:

$$\mathcal{F}_{\rm KLS}(q^2) = \sum_N \frac{(-1)^N(2L+1)!!}{(2N)!!(2L+2N+1)!!}(qR/\hbar)^{2N}\mathcal{F}^{(N)}_{\rm KLS}. \tag{5}$$

Because $qR/\hbar \ll 1$ is for typical β decays, the leading contributions come essentially from the first few form factor coefficients $\mathcal{F}^{(N)}_{\rm KLS}$ [2].

In practice the shape factor $C(w_{\rm e})$ as a whole can be expressed as a power series in the small quantities $\eta_{i=1,2,3,4,5} = \alpha Z$, $p_{\rm e}R/\hbar$, $qR/\hbar$, $m_{\rm e}cR/\hbar$, and $W_{\rm e}R/\hbar c$. Excluding the prefactors dependent on the integers $k_{\rm e}, k_\nu$, and K the functions $M_K(k_{\rm e},k_\nu)$ and $m_K(k_{\rm e},k_\nu)$ appearing in Eq. (4) thus consist of the terms $\prod_i \eta_i^{\alpha_i} \times \mathcal{F}^{(N)}_{\rm KLS}$ with $\alpha_i = 0,1,2,\ldots$. Furthermore, the summation of Eq. (4) is restricted to two distinct cases: For a given level of forbiddeness K one only needs to add up the terms that satisfy $k_{\rm e}+k_\nu = K+1$ and $k_{\rm e}+k_\nu = K+2$. In the earlier applications (see, e.g., [30–32,34]) only the first-order terms in Eq. (4) are taken into account. These are the ones related to the lowest powers of the small quantities η_i, i.e., terms $\prod_i \eta_i^{\alpha_i} = (p_{\rm e}R/\hbar)^{k_{\rm e}-1}(qR/\hbar)^{k_\nu-1}$ and $(p_{\rm e}R/\hbar)^{k_{\rm e}-1}(qR/\hbar)^{k_\nu-1}\eta_j$ for the summation $k_{\rm e}+k_\nu = K+1$ and only $(p_{\rm e}R/\hbar)^{k_{\rm e}-1}(qR/\hbar)^{k_\nu-1}$ for $k_{\rm e}+k_\nu = K+2$. It is worth noting that in this case the formalism for unique decays with the change of angular momentum equal to $K+1$ is drastically simplified because only one term of Eq. (4) is nonvanishing and contributes to the decay probability.

When the shape factor is cut by these order-of-magnitude considerations the remaining form-factor coefficients can be related to the nuclear matrix elements (NMEs). This is done by assigning

$${}^{V/A}F^{(N)}_{\rm KLS}(k_{\rm e},m,n,\rho) = (-1)^{K-L}\,{}^{V/A}\mathcal{M}^{(N)}_{\rm KLS}(k_{\rm e},m,n,\rho). \tag{6}$$

In this way all the NMEs with superscript A carry a prefactor $\lambda = g_{\rm A}/g_{\rm V}$. These are the vector (V) and axial-vector (A) coupling constants that were used to re-normalize the hadronic current. The appearance of these constants in Eq. (4) modulates the effect of the NMEs. When the value of $g_{\rm A}$ is increased the impact of the corresponding NMEs increases. The exact opposite happens when the value is decreased.

The NMEs for a transition between an initial (i) and a final (f) nuclear state can be decomposed as

$${}^{V/A}\mathcal{M}^{(N)}_{\rm KLS} = \frac{1}{\sqrt{2J_i+1}}\sum_{pn} {}^{V/A}m^{(N)}_{\rm KLS}(pn)(\psi_f||[c^\dagger_p\tilde{c}_n]_K||\psi_i), \tag{7}$$

where the summation runs over the different proton (p) and neutron (n) model-space single-particle states. The single-particle matrix elements ${}^{V/A}m^{(N)}_{\rm KLS}(pn)$ are model independent, and in this work they are calculated using relativistic nuclear single-particle wave functions. These wave functions are written as

$$\phi_{nljm}(\mathbf{r}) = \begin{pmatrix} G_{nljm}(\mathbf{r}) \\ F_{nljm}(\mathbf{r}) \end{pmatrix}, \tag{8}$$

where $G_{nljm}(\mathbf{r})$ are the large and $F_{nljm}(\mathbf{r})$ the small components of the four spinor. These components are the same as those used in Ref. [34], i.e.,

$$G_{nljm}(\mathbf{r}) = i^l g_{nl}(r)\left[Y_l\chi_{\frac{1}{2}}\right]_{jm}, \tag{9a}$$

$$F_{nljm}(\mathbf{r}) = \frac{\boldsymbol{\sigma}\cdot\mathbf{p}}{2M_Nc}G_{nljm}(\mathbf{r}), \tag{9b}$$

where $g_{nl}(r)$ are taken to be the radial parts of the harmonic-oscillator wave functions. The one-body transition densities (OBTDs) $(\psi_f||[c^\dagger_p\tilde{c}_n]_K||\psi_i)$, on the other hand, need to be calculated from a nuclear-structure model. In this work both MQPM and NSM are used to describe the initial- and final-state wave functions. The explicit expressions for the derivation of the OBTDs from the MQPM wave functions are found, e.g., in Ref. [34], while the corresponding NSM quantities are computed using the computer code NUSHELLX [28].

In the present work we increase the accuracy of the shape function (4) by going beyond the above-described lowest-power expansion and add the second-order terms, i.e., $(pR/\hbar)^{k_{\rm e}-1}(qR/\hbar)^{k_\nu-1}\eta_j\eta_k$ for the $k_{\rm e}+k_\nu = K+1$ and $(pR/\hbar)^{k_{\rm e}-1}(qR/\hbar)^{k_\nu-1}\eta_j$ for $k_{\rm e}+k_\nu = K+2$. This way the number of NMEs involved in the calculations increases drastically. In the case of fourth-forbidden nonunique decays the number NMEs is increased from 12 to 45. As a rule of thumb the second-order terms involve matrix elements that are taken from the first-order NMEs (for all of these $N=0$) by adding an extra factor of $(r/R)^{2N}$ to the integrands of the first-order single-particle matrix elements [1]. However, for several terms the higher-degree Coulombic factors are also taken into account. The relevant factors are tabulated, e.g., in Ref. [2].

It should be noted that we do not consider the radiative corrections of Coulomb interaction in the current work. Neither are the actual electron screening corrections included in the theory. The latter corrections stem from the interaction between the emitted β particle and the atomic electrons, and are generally considered important only for very low Q-value decays. For example, in Ref. [31] an effect of only less than 1% to the decay half-life was observed in the β^- decay of ^{48}Ca with a ground-state-to-ground-state Q value of 278 ± 5 keV. It can be further argued that these corrections contribute more to electron-capture (EC) decay and much less to the β^- one [2].

III. NUMERICAL APPLICATION OF THE FORMALISM

The basic procedures involved in the application of the MQPM theory, using a realistic Bonn one-boson exchange potential with the G-matrix techniques, is described, e.g., in Ref. [27]. Its recent application on the β decay branches of ^{115}Cd can be found in Ref. [30]. Following the guidelines of Ref. [26], where the work was previously carried out, we chose to perform the calculations using an extensive valence space of

orbitals $1p - 0f - 2s - 1d - 0g - 0h$ for both of the protons and neutrons in the reference nuclei ^{112}Cd and ^{116}Sn. The adopted parametrization for the Coulomb-corrected Woods-Saxon potential was the one by Bohr and Mottelson [35].

In each case some of the computed Woods-Saxon single-particle energies were slightly modified to improve the quality of the BCS one-quasiparticle spectra. The aim of this adjustment was to fit the lowest one-quasiparticle states closer to the experimental ones. Some further phenomenological fine tuning was likewise applied to the QRPA calculations. In practice this was implemented by scaling the particle-particle and particle-hole interaction matrix elements separately by parameters $g_{\rm pp}$ and $g_{\rm ph}$ for each of the few lowest multipoles. At the very last step the total amount of basis states involved in the subsequent MQPM calculations was restricted by introducing a 3.0-MeV cutoff energy for the QRPA states.

The shell-model OBTDs were calculated with an inert core ^{78}Ni by taking proton orbitals $1p_{3/2}$, $0f_{5/2}$, $1p_{1/2}$, $0g_{9/2}$ and neutron orbitals $0g_{7/2}$, $1d_{5/2}$, $1d_{3/2}$, $2s_{1/2}$, $0h_{11/2}$. We performed calculations with the NSM code NUSHELLX [28] and effective interaction jj45pna [36,37] which is a CD-Bonn potential, re-normalized using the perturbative G-matrix approach. This interactions has four parts, corresponding to the neutron-neutron, neutron-proton and proton-proton nuclear force, and the Coulomb repulsion between the protons. Recently the shell-model results with the jj45pna interaction for $^{122-126}$Ag were reported in Ref. [37].

Because of the large dimensions involved in the present NSM calculation we had to enforce a controlled truncation of the neutron configurations. For the $A = 113$ nuclei we forced complete filling of the $0g_{7/2}$ orbital and allowed no neutron excitations to the $0h_{11/2}$ orbital. In the case of ^{115}In and ^{115}Sn we opened the $0g_{7/2}$ orbital for excitations, but still did not allow neutron excitations to the $0h_{11/2}$ orbital. With these truncations the present NSM calculations manage to predict correctly the ground state for ^{113}Cd as $1/2^+$ $(\nu s^1_{1/2})$ and $9/2^+(\pi g^{-1}_{9/2})$ for ^{113}In. Similarly for ^{115}In we predict correctly the ground state as $9/2^+(\pi g^{-1}_{9/2})$ and for ^{115}Sn the ground state as $1/2^+$ $(\nu s^1_{1/2})$.

IV. RESULTS

Below we present the results of our calculations concerning the β-decay half-lives and β spectra of the two exemplary fourth-forbidden nonunique ground-state-to-ground-state β^- transitions in ^{113}Cd and ^{115}In.

A. General features of the β-decay half-lives

The MQPM and NSM computed partial half-lives for the fourth-forbidden nonunique β^--decay branches of ^{113}Cd and ^{115}In, without and with the second-order corrections to the shape function, are presented in Fig. 1. The partial half-lives are plotted as functions of the axial-vector coupling constant $g_{\rm A}$, and a comparison with experiment is performed by drawing the experimental values, with their experimental errors included, as horizontal shaded stripes in the same figures. In this analysis we keep the vector coupling constant in its CVC value $g_{\rm V} = 1.0$. It is interesting to note that in each case there are actually two crossing points with the experiment. The larger effective values of $g_{\rm A}$ are found to be close to the bare nucleon value, whereas the more strongly quenched results are in the less-than-unity range. The extracted values are all tabulated in Table I. This table, together with Fig. 1, shows that the effects of the second-order terms appear to be relatively small when only the partial half-lives are considered.

TABLE I. Values of $g_{\rm A}$ which reproduce the experimental partial half-lives for the decay branches of Fig. 1. The results are tabulated for both the MQPM and the NSM, and for the two cases of including (the rows with 2nd) and excluding (1st) the second-order terms in the shape factor. Both the lower-than-unity and higher-than-unity values of $g_{\rm A}$ are tabulated.

		Effective $g_{\rm A}$			
Nuclear model	Order	^{113}Cd		^{115}In	
MQPM	1st	0.28	1.46	0.76	1.16
	2nd	0.27	1.45	0.75	1.15
NSM	1st	0.61	1.33	0.58	1.24
	2nd	0.60	1.32	0.57	1.23

It should be noted that, although the choice $g_{\rm A} \simeq 1$ is considered to be the more conservative alternative for the effective value of the coupling constant, much stronger quenching is many times recorded in other studies (check, e.g., Refs. [6,7,9–11,13,17,18] pertaining to either allowed or first-forbidden unique decays. In Ref. [13] a systematic examination of the Gamow-Teller β^- and EC decay branches within the mass range $A = 100$–136 yields consistently less than unity values for $g_{\rm A}$ for all the examined decay branches. The same is essentially true also in the other studies mentioned. The question then arises whether the same type of effective values of $g_{\rm A}$ are needed to reproduce decay transitions of higher forbiddeness.

In all the mentioned earlier studies only one physical observable per decay transition was considered. The β-spectrum shape could not be used as another observable because of the universal structure of the involved shape functions. In the current work we consider nonunique forbidden decay channels where no universal shape of the β spectrum occurs because now the complicated dependence on the angular momentum transfer allows for a much more complex expression for the β-decay shape factor of Eq. (4). The shape factor, and thus the inverse half-life, attains the form of a second-order polynomial, i.e., $(t_{1/2})^{-1} \propto c_1 \times g_{\rm A}^2 + c_2 \times g_{\rm A} + c_3$, in terms of $g_{\rm A}$. The general behavior of the quantity $t_{1/2}$ as a function of the coupling constant becomes then exactly the bell-shaped curve depicted in Fig. 1. A total of two crossing points with the experiment can be found from the nonzero first-order term c_2. In contrast to this the general shape factor for the allowed decays is $b_1 \times g_{\rm A}^2 + b_2$ [38]. If only Gamow-Teller decays are considered, then $t_{1/2} \propto 1/g_{\rm A}^2$ holds directly, as also happens for the forbidden unique decays [38]. Thus, only one solution with a positive value of $g_{\rm A}$ is available in these cases.

The previous half-life analyses can be extended to the case of a freely varying value of the vector coupling constant $g_{\rm V}$. To enable a clear-cut access to the effects of the simultaneous

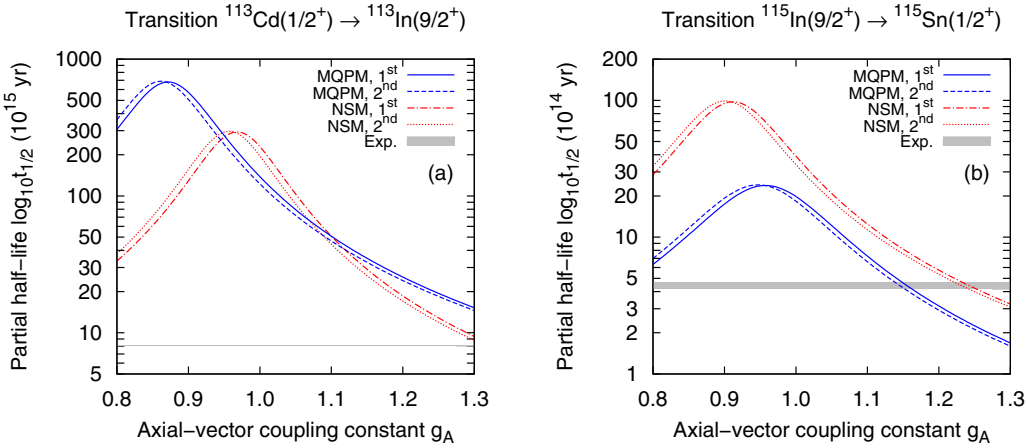

FIG. 1. MQPM and NSM computed partial half-lives of the fourth-forbidden nonunique ground-state-to-ground-state β^--decay branches of ^{113}Cd (a) and ^{115}In (b) as functions of the value of the axial-vector coupling constant g_A. The value $g_V = 1.0$ was adopted in the calculations. The notation 1st (2nd) refers to inclusion of the first-order (both the first- and second-order) terms of the shape factor. Experimental half-lives are given as gray horizontal areas in the same figures.

variation of the values of both g_V and g_A we can inspect the contributions of the vector (V) and axial-vector (A) dependent terms to the integrated shape factor (3). It can be decomposed into a form,

$$\tilde{C} = g_V^2 \tilde{C}_V + g_A^2 \tilde{C}_A + g_V g_A \tilde{C}_{VA}, \qquad (10)$$

where the coupling-constant independent coefficients $\tilde{C}_V$, $\tilde{C}_A$, and $\tilde{C}_{VA}$ are tabulated in Table II. It can be seen that the contributions coming from the vector and axial-vector parts are of the same sign and order, and that in each case the cross term $\tilde{C}_{VA}$ is roughly twice as large as the vector and axial-vector parts and of opposite sign. Thus much of the contribution coming from the first two terms is canceled out by the cross term. This is strikingly seen in the last line of Table II where the value of the total integrated shape factor is given for $g_V = g_A = 1.0$, i.e., it is directly the sum of the three terms above it in the table. Furthermore, it can be seen that the second-order terms affect essentially only the vector part of the shape factor. Considering the results of Fig. 1 and Table II the most decisive part of the theory is well contained in the NMEs of the first-order terms.

TABLE II. The vector ($\tilde{C}_V$), axial-vector ($\tilde{C}_A$), and vector-axial-vector ($\tilde{C}_{VA}$) dependent terms of the integrated shape factor. Again the computed results are presented both including (the columns with 2nd) and excluding (1st) the second-order terms of the shape factor. The values on the fourth row correspond to the sum of the three components, i.e., the total integrated shape factor for $g_V = g_A = 1.0$. All the values are given in units of 10^{-21}.

	MQPM		NSM	
Factor	1st	2nd	1st	2nd
$\tilde{C}_V$	52.064	50.857	171.762	167.834
$\tilde{C}_A$	68.146	68.146	182.544	182.544
$\tilde{C}_{VA}$	−118.801	−117.413	−353.457	−349.385
$\Sigma\tilde{C}_i$	1.409	1.590	0.849	0.993

In Fig. 2 we study the effects of the variation of the value of g_V on the β-decay half-life. First of all, in Fig. 2 it is evident that the shift in the value of g_V results in a shift in the half-life curve, roughly preserving its shape and only altering its peak height. Even more interestingly, the half-life of the ^{113}Cd decay transition is peaked whenever roughly equal values of the two coupling constants are used. The (universal) symmetry of the half-life curves indicates that the experimental half-life is obtained for an infinite number of (g_V,g_A) pairs by increasing or decreasing the value of g_A by roughly three units relative to a given value of g_V. Similar results are obtained for the ^{115}In decay. This means that the half-life analysis alone is not able to determine uniquely the values of g_V and g_A when their

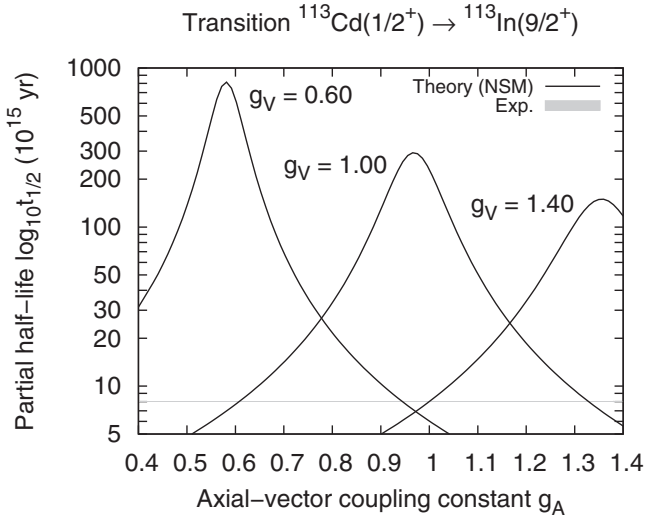

FIG. 2. NSM computed partial half-lives of the fourth-forbidden nonunique ground-state-to-ground-state β^--decay branch of ^{113}Cd as functions of the value of the axial-vector coupling constant g_A for selected values of g_V. Both the first-order and second-order terms of the shape factor are taken into account in the results. The experimental half-life is given as a gray horizontal stripe in the same figure.

values are allowed to vary freely. The situation is changed drastically when the inspection of the shape of the β spectrum is introduced, as shown in the following subsection.

B. General features of the β-decay electron spectra

The nontrivial structure of the shape function for forbidden nonunique β decays opens up a potential extra route to investigate the effective values of the weak coupling constants $g_{\rm V}$ and $g_{\rm A}$. As mentioned in the introduction, we call this analysis tool the spectrum-shape method. The viability of this method depends on how sensitive the β-spectrum shape is to the values of $g_{\rm V}$ and $g_{\rm A}$. To have a feeling of the sensitivity of the spectrum to $g_{\rm A}$ in our two exemplary cases we keep the CVC value $g_{\rm V} = 1.0$ of the vector coupling constant and plot for the exemplary cases the integrand of Eq. (3) as a function of the electron energy for several values of $g_{\rm A}$. The results are given in Fig. 3. To draw attention to the changes in the shape of the spectra itself we chose to normalize the areas under each of the curves to unity. As it can be seen from these figures the spectrum shape is very strongly dependent on the adopt value of the coupling constant $g_{\rm A}$, showing the power of SSM. Furthermore, it can be seen that the inclusion or exclusion of the second-order terms also contributes to the spectral shape. This effect is slightly more conspicuous when looking at the actual values of the integrands without the unity normalization.

A closer look at Fig. 3 shows that in each case the behavior of the spectrum shape is very similar. At low values, i.e., $g_{\rm A} < 0.8$, the spectrum shape resembles that of a single downward slope. The most interesting behavior starts to occur when $g_{\rm A}$ verges on the unity. At these values there is a formation of a very distinct maximum point at the midsection of the spectra. At the values greater than unity the mid-maximum starts to vanish, and when the value of $g_{\rm A}$ is further increased the spectra again attain the shape of a single downward slope. It is worth noting that values of $g_{\rm A}$ with most notable mid-maximum points coincide with the partial half-life maxima of Fig. 1. That is, the partial half-lives of the two transitions are at their longest when these particular values of $g_{\rm A}$ are used. The observed behavior can be related to the actual values of the shape factors. In these cases the NMEs are multiplied by $g_{\rm A}$ in a way that the integrand of Eq. (3) yields overall the lowest values.

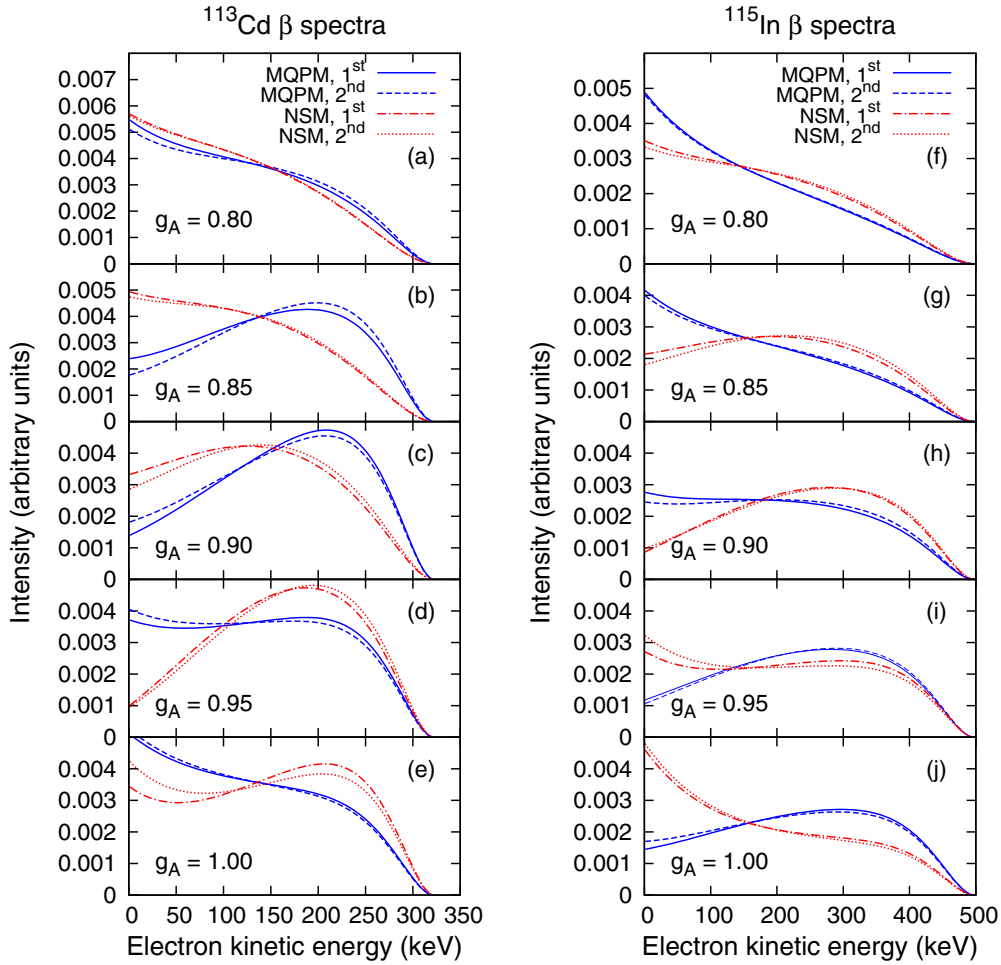

FIG. 3. β spectra of the two fourth-forbidden decay branches of ^{113}Cd (a)–(e) and ^{115}In (f)–(j) for $g_{\rm V} = 1.0$. The spectra are plotted using several values of $g_{\rm A}$ and they include results from both the MQPM and NSM nuclear models. Areas under each of the curves are normalized to unity.

In the case of ^{113}Cd the NMEs are larger for the MQPM than for the NSM. Thus in the case of the half-lives the extreme values of g_A are extracted from the MQPM calculations as shown in Table I. The NSM predicts less drastic effective values of g_A. For ^{115}In, on the other hand, the situation is completely reversed. In that case the extreme values of g_A stem from the NSM calculations. However, although the two nuclear models and model spaces used in the calculations are very different the overall results emerging from the two models still seem to be somewhat similar. Even the half-life peaks in Fig. 1 seem to be shifted only by 0.05–0.1 units in the value of g_A. A similar shift is also visible in the behavior of the β spectra in Fig. 3. Extension of the present pilot study to other nuclear transitions and other nuclear models would certainly shed light on the model dependence of the effective value of g_A in nuclear-structure calculations.

Extending the previous spectrum-shape analysis to the free variation of g_V is somewhat straightforward: Taking different combinations of the (g_V, g_A) pairs and recording the emerging spectrum shape leads to the general overall observation that the number of possible (g_V, g_A) combinations that reproduces the experimental spectrum shape, discussed in the following subsection, is drastically reduced. The key feature in this is that the humped structure of the β spectrum, visible in the region $g_A \sim 0.85$–1.00 for ^{113}Cd and in the region $g_A \sim 0.90$–1.00 for ^{115}In in Fig. 3, is obtained only when the two coupling constants have roughly the same value. For values of g_V and g_A differing more than 10% the spectrum shape becomes a dull monotonously decreasing curve.

C. Extraction of the effective values of the weak coupling constants

To assess the very intriguing possibility of extracting the effective value of g_A (and possibly g_V) by using SSM, we performed a comparison with the available experimental data of Belli *et al.* [29] for the ^{113}Cd β spectrum by including also the second-order terms. It should immediately be noted that the experimentally measured Q value in that study is 343.1 ± 0.6 keV. Thus, it differs from the more established value of 322 ± 1 keV [25] that is used in the present work. To allow for the comparison between the computed β spectrum and the data the theoretical β spectra were recalculated using the Q value 343.1 ± 0.6 keV of Ref. [29]. We start by keeping the canonical value $g_V = 1.0$. The results are presented in Fig. 4. As it can be seen the shell model succeeds in providing an excellent match with the experiment when the value of the axial coupling is taken to be $g_A = 0.90$. For the MQPM the match is not as perfect, but a relatively close match can be found at around $g_A = 0.83$. Again, the areas under both the theoretical and the experimental curve are normalized to unity.

Despite the fact that SSM allows for the extraction of the effective values of g_A within the range deduced from the half-life, there is a notable contradiction between the results that these methods provide. The values of g_A, suggested by SSM, fall in the middle of the extreme values of g_A, suggested by the half-life method. Thus, for $g_V = 1.0$, it is not possible to decide whether the effective value of g_A is closer to its bare value or the strongly quenched value. More experimental data on these type of decay transitions are needed to perform a more systematic study. One particular problem of the experiments is to extract the β spectrum below 100 keV. Thus one can expect notable uncertainties in the low-energy β spectra of the current experiments. To render SSM its full power, a systematic improvement and extension of the future experiments is thus called for.

It is interesting to see if the above conclusions remain valid when the value of the vector coupling constant g_V is allowed to vary around its CVC value $g_V = 1.0$. As mentioned at the end of Sec. IV B the humped shape of the experimental β spectrum in Fig. 4 is only attained when the values of g_V and g_A are sufficiently close to each other. According to the current results (see Fig. 5) the shape of the experimental β spectrum is well reproduced when (a) the difference between the values of g_V and g_A is equal to 0.1, and (b) both values are close to unity. If either one of the coupling constants is more drastically

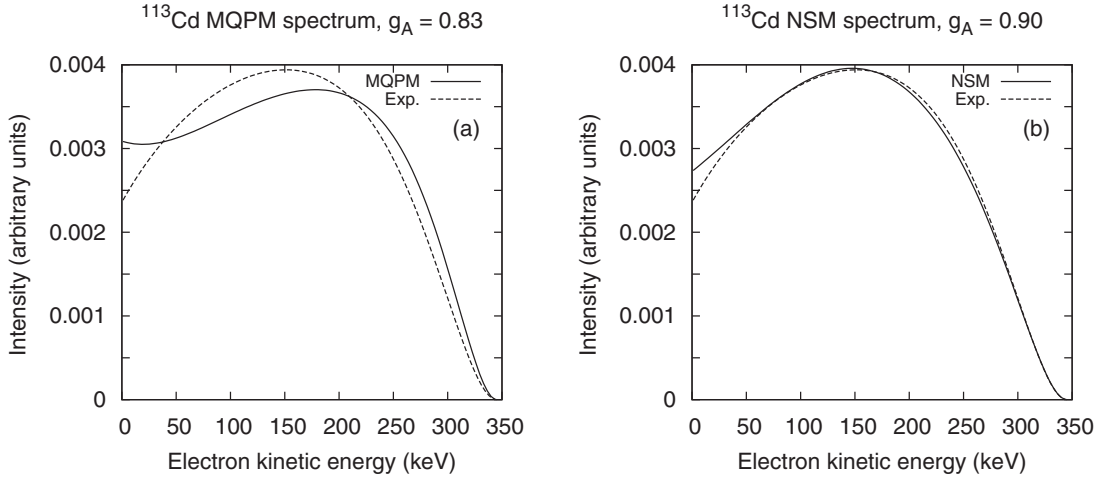

FIG. 4. Computed β spectra of the fourth-forbidden ^{113}Cd β^- branch compared with the experiment. The second-order terms have been included in the computations and only the best matches are shown in the figure. The canonical value $g_V = 1.0$ is used in the calculation. The experimental data are from Ref. [29], and the theoretical β spectra had to be recalculated by using the Q value adopted in that study.

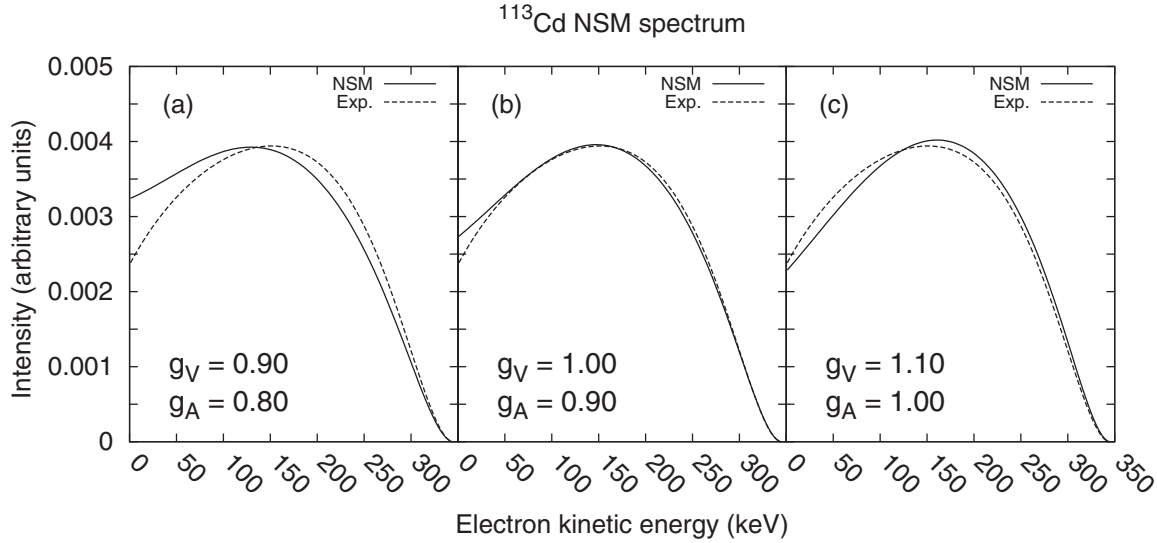

FIG. 5. NSM computed β spectra of the fourth-forbidden ^{113}Cd β^- branch compared with the experimental spectrum when also the value of g_V is varied. The second-order terms have been included in the computations and only the region of best match with the experiment is illustrated in the figure.

quenched the agreement with the experiment is sharply lost and the computed β spectra swiftly acquire the shape of a monotonously decreasing curve. Therefore it should be noted that although the predicted partial half-life can be brought down to match the experimental value by the quenching of g_V the inspection on the shape of the β spectra strongly contradicts these quenched choices of g_V values. For the presently used nuclear models, inspection of the β spectra for different values of the pairs (g_V, g_A) leads to the conclusion that the values $g_V = 1$ (the CVC value of g_V) and $g_A = 0.9$ bring the β spectrum closest to the currently available experimental data. This best matching is displayed in the middle panel of Fig. 5 for the NSM.

Finally, it is interesting to speculate about the possible reason(s) for the contradictory half-life and spectrum-shape results of the present pilot study. If the entire half-life curves of Fig. 1 were brought down by suitable values of the NMEs, then in the extreme case of only one touching point with the experiment the two methods practically yield the same effective values of g_A for the ^{113}Cd decay. Hence, it can be argued that the discrepancies between the results of the two methods are related to the inaccuracies in the nuclear-structure calculations.

It is reasonable to expect that a successful description of the nucleus and its decay processes can make the half-life and spectrum-shape sets of results to coincide. Special care must, however, be also taken when assessing the quality of the experimental data. The energy resolution in Ref. [29] is relatively low, and some alteration of the β spectrum at low energies (below 50–100 keV) is not excluded when more precise data becomes available. This is a crucial improvement because it is the low-energy part of the β spectrum that depends very strongly on the value of g_A (and g_V, keeping in mind the need for close-by values of the two coupling constants). Regrettably this is also the part where most difficulties in the experimental work occur.

V. CONCLUSIONS

In this article we have conducted a pilot study on the possibility of using β spectra of forbidden nonunique β-decay transitions to access the effective values of weak coupling constants g_V (vector) and g_A (axial vector) in nuclear-model calculations. We coin this method the spectrum-shape method. This method is complementary to the derivation of g_A values through measured β-decay half-lives. The complex dependence of the shape function of the forbidden nonunique β-decay transitions on g_A (and g_V), the phase-space factors, and the nuclear matrix elements makes the shape of the computed β spectrum depend on g_A (and g_V) in a highly nontrivial way. Computing the β spectrum for different values of g_V and g_A and comparing with the measured spectrum can give information on the effective values of these coupling constants. The potential of SSM depends on the sensitivity of the β-spectrum shape to the values of g_V and g_A.

To access the sensitivity of the β spectrum to g_V and g_A we have studied in this work two exemplary forbidden nonunique β^--decay transitions, namely the fourth-forbidden nonunique ground-state-to-ground-state β-decay branches of ^{113}Cd and ^{115}In by using the microscopic quasiparticle-phonon model and the nuclear shell model. We have also added the usually omitted second-order terms in the computed shape function to see their effect on the half-life and shape function. It turned out that the second-order terms have a negligible effect on the half-life but noticeable effect on the shape of the β spectrum in both nuclear models. Furthermore, the two exemplary cases showed a very high sensitivity of the β-spectrum shape to the values of g_V and g_A for both nuclear models, rendering SSM potentially a very powerful tool for determination of the effective value of these two coupling constants. In both nuclear models the sensitivity was found to be strongest, for a given value of g_V, close to the value of g_A that corresponds to the longest computed partial half-life.

The computed β-spectrum shape could be compared with the measured one of Ref. [29] for ^{113}Cd. The comparison revealed that an excellent agreement with the experiment is obtained with the values $g_V = 1.0$ and $g_A = 0.90$ in the case of NSM. The agreement was not as perfect in the case of MQPM but a relatively close resemblance was found with $g_V = 1.0$ and $g_A = 0.83$. Contrariwise, the comparison of the quadratic dependence of the theoretical decay half-life on g_A with half-life data produced two values of g_A, either highly quenched or unquenched. The contradicting results of SSM and half-life analyses are most likely associated with the deficiencies in the nuclear-structure calculations and more calculations with different nuclear Hamiltonians and different nuclear-structure frameworks are called for in the future. At this point it is important to note that the contradiction between the SSM and half-life results is not rectified in any obvious way by the quenching of the vector coupling constant g_V as it happens in some other studies involving β decays of low forbiddeness. Although in practice the half-lives can be brought down to experiment by either raising or lowering the value of g_V, the match between the predicted and the experimental β spectra is lost in the process. Interestingly, the present inspection using the ^{113}Cd data seems to strongly favor the choice $g_V \approx 1$ in accordance with the CVC hypothesis of the standard model [8].

More experimental data are needed on the electron-spectrum shapes of the nonunique β-decay transitions of various degrees of forbiddeness to facilitate a systematic study of the effective value of g_A (and g_V) in various nuclear models. A particular experimental challenge in the future is to obtain accurate enough data on the spectrum shape at low electron energies, below 50–100 keV, to fully exploit the power of SSM.

ACKNOWLEDGMENTS

This work was partly supported by the Academy of Finland under the Finnish Center of Excellence Program 2012-2017 (Nuclear and Accelerator Based Program at JYFL). M.H. was supported by a graduate student stipend from the Finnish Cultural Foundation. We want to thank V. I. Tretyak and his colleagues (Ref. [29]) for providing the experimental β-spectrum data of ^{113}Cd.

[1] H. F. Schopper, *Weak Interactions and Nuclear Beta Decay* (North-Holland, Amsterdam, 1966).
[2] H. Behrens and W. Bühring, *Electron Radial Wave Functions and Nuclear Beta-decay* (Clarendon Press, Oxford, 1982).
[3] A. Bohr and B. R. Mottelson, Phys. Lett. B **100**, 10 (1981).
[4] J. Suhonen and O. Civitarese, Phys. Rep. **300**, 123 (1998).
[5] J. Maalampi and J. Suhonen, Adv. High Energy Phys. **2013**, 505874 (2013).
[6] H. Ejiri, N. Soukouti, and J. Suhonen, Phys. Lett. B **729**, 27 (2014).
[7] H. Ejiri and J. Suhonen, J. Phys. G: Nucl. Part. Phys. **42**, 055201 (2015).
[8] E. D. Commins, *Weak Interactions* (McGraw-Hill, New York, 1973).
[9] A. Faessler *et al.*, J. Phys. G: Nucl. Part. Phys. **35**, 075104 (2008).
[10] J. Suhonen and O. Civitarese, Phys. Lett. B **725**, 153 (2013).
[11] J. Suhonen and O. Civitarese, Nucl. Phys. A **924**, 1 (2014).
[12] D. S. Delion and J. Suhonen, Eur. Phys. Lett. **107**, 52001 (2014).
[13] P. Pirinen and J. Suhonen, Phys. Rev. C **91**, 054309 (2015).
[14] B. H. Wildenthal, M. S. Curtin, and B. A. Brown, Phys. Rev. C **28**, 1343 (1983).
[15] G. Martínez-Pinedo, A. Poves, E. Caurier, and A. P. Zuker, Phys. Rev. C **53**, R2602 (1996).
[16] E. Caurier, F. Nowacki, and A. Poves, Phys. Lett. B **711**, 62 (2012).
[17] J. Barea, J. Kotila, and F. Iachello, Phys. Rev. C **87**, 014315 (2013).
[18] J. Barea, J. Kotila, and F. Iachello, Phys. Rev. C **91**, 034304 (2015).
[19] J. Suhonen and O. Civitarese, J. Phys. G: Nucl. Part. Phys. **39**, 085105 (2012).
[20] J. Suhonen and O. Civitarese, J. Phys. G: Nucl. Part. Phys. **39**, 124005 (2012).
[21] E. K. Warburton, Phys. Rev. C **42**, 2479 (1990).
[22] E. K. Warburton, Phys. Rev. C **44**, 233 (1991).
[23] T. Suzuki, T. Yoshida, T. Kajino, and T. Otsuka, Phys. Rev. C **85**, 015802 (2012).
[24] Q. Zhi, E. Caurier, J. J. Cuenca-García, K. Langanke, G. Martínez-Pinedo, and K. Sieja, Phys. Rev. C **87**, 025803 (2013).
[25] ENSDF at NNDC site, http://www.nndc.bnl.gov/
[26] M. T. Mustonen and J. Suhonen, Phys. Lett. B **657**, 38 (2007).
[27] J. Toivanen and J. Suhonen, Phys. Rev. C **57**, 1237 (1998).
[28] B. A. Brown, W. D. M. Rae, E. McDonald, and M. Horoi, Computer code NUSHELLX, Michigan State University, East Lansing.
[29] P. Belli, R. Bernabei, N. Bukilic, F. Cappella, R. Cerulli, C. J. Dai, F. A. Danevich, J. R. de Laeter, A. Incicchitti, V. V. Kobychev, S. S. Nagorny, S. Nisi, F. Nozzoli, D. V. Poda, D. Prosperi, V. I. Tretyak, and S. S. Yurchenko, Phys. Rev. C **76**, 064603 (2007).
[30] M. Haaranen and J. Suhonen, Eur. Phys. J. A **49**, 93 (2013).
[31] M. Haaranen, M. Horoi, and J. Suhonen, Phys. Rev. C **89**, 034315 (2014).
[32] M. Haaranen, P. C. Srivastava, J. Suhonen, and K. Zuber, Phys. Rev. C **90**, 044314 (2014).
[33] K. L. G. Heyde, *The Nuclear Shell Model* (Springer, Berlin, 1990).
[34] M. T. Mustonen, M. Aunola, and J. Suhonen, Phys. Rev. C **73**, 054301 (2006).
[35] A. Bohr and B. R. Mottelson, *Nuclear Structure* (Benjamin, New York, 1969), Vol. I.
[36] R. Machleidt, Phys. Rev. C **63**, 024001 (2001).
[37] S. Lalkovski *et al.*, Phys. Rev. C **87**, 034308 (2013).
[38] J. Suhonen, *From Nucleons to Nucleus: Concepts of Microscopic Nuclear Theory* (Springer, Berlin, 2007).